A cold frontal life cycle climatology and front–cyclone relationships over the North Atlantic and Europe

International Journal of Climatology

International Journal of Climatology RMetS

RESEARCH ARTICLE OPEN ACCESS

A Cold Frontal Life Cycle Climatology and Front–Cyclone Relationships Over the North Atlantic and Europe

Tobias Lichtenegger[1] | Armin Schaffer[1] | Albert Ossó[1] | Oscar Martínez-Alvarado[2,3] | Douglas Maraun[1]

[1]Wegener Center for Climate and Global Change, University of Graz, Graz, Austria | [2]Department of Meteorology, University of Reading, Reading, UK | [3]National Centre for Atmospheric Science, University of Reading, Reading, UK

Correspondence: Tobias Lichtenegger (tobias.lichtenegger@uni-graz.at)

Received: 7 October 2024 | **Revised:** 15 January 2025 | **Accepted:** 4 March 2025

Funding: This work was supported by Austrian Science Fund (I 4831-N).

Keywords: climatology | cold fronts | detection | extratropical cyclones | life cycle | tracking

ABSTRACT

Atmospheric fronts and cyclones play an important role in day-to-day weather variability, especially in the mid-latitudes and during the winter season. Severe rainfall and windstorm events are often associated with the passage of a front or a cyclone. While there are many studies of individual fronts and climatologies of instantaneous fronts, there is no climatological study considering the whole frontal life cycle over time. Therefore, we use a front and cyclone tracking algorithm, together with a widely used front detection method, to detect and track cold fronts and cyclones over the North Atlantic and Europe in the extended winter season (October–March) in the ERA5 reanalysis data set. This enables a climatological study providing statistics of the frontal life cycle based on thousands of fronts. Several life cycle characteristics and frontal parameters are defined to investigate the frontal life cycle and the conditions and processes in the frontal region. Fronts are linked to their parent cyclone to study relationships between frontal and cyclonic properties. Cold fronts primarily develop over the Western North Atlantic and are found to decay at or soon after landfall on the European coast in most cases. Cold fronts tracked over the North Atlantic are found to last over 1 day longer and travel up to 1500 km farther on average than cold fronts tracked over the Mediterranean and over land. Cold frontal life cycle characteristics are strongly dependent on the North Atlantic Oscillation, with cold fronts appearing in a positive phase lasting longer and travelling faster and farther. Stronger cyclones are related to stronger frontal wind speeds at the surface as well as in the cold and warm sectors. The relationships between frontal and cyclonic properties are found to weaken over the course of their life cycle.

1 | Introduction

Atmospheric fronts and extra-tropical cyclones (hereafter referred to as cyclones) are strongly interacting phenomena of the atmospheric general circulation and are responsible for the day-to-day variability of the weather in the mid-latitudes, as they move large quantities of moisture, heat, and momentum. Over Europe during the winter season, up to 90% of total precipitation is found to be associated with cyclones (Hawcroft et al. 2012) and 10%–50% of total precipitation has been directly attributed to cold fronts (Catto et al. 2012). Extreme precipitation is even more strongly associated with cold fronts (Catto and Pfahl 2013) and has been linked to the humidity content and transport, as well as the meso-scale circulation at the front (Schaffer et al. 2024). Cyclones are also known to cause extreme wind speeds (Gramcianinov et al. 2020; Dowdy and Catto 2017; de Ponce León and Guedes Soares 2014; Owen et al. 2021), which can lead to substantial socioeconomic impacts (Easterling et al. 2000). Dowdy and Catto (2017) found that the combination of cyclones and fronts has the largest contribution to extreme precipitation and extreme surface winds in the mid-latitudes.

Cyclones and atmospheric fronts are closely linked phenomena. Fronts are known as elongated regions of high temperature, humidity, and pressure gradients, marking the boundary of different air masses. Descriptive and theoretical discussions on frontogenetic mechanisms are given in e.g. Lamb (1951), Hoskins (1982) and Davies (1999). These fronts are the main breeding points for the formation of cyclones when an upper-level disturbance moves over a preexisting front and triggers a frontal wave. Conceptual models of the following life cycle of the cyclone and its associated cold and warm fronts have been developed by most notably Bjerknes and Solberg (1922) and Shapiro (1990). Later, Hewson (2009) extended this theory by also incorporating the life cycle stages prior to the formation of a vigorous cyclone.

Climatological studies of the life cycle of cyclones in the mid-latitudes have been conducted for at least the last two decades (e.g., Pinto et al. 2005; Wernli and Schwierz 2006; Dacre and Gray 2009; Ulbrich et al. 2009; Neu et al. 2013; Heitmann et al. 2024), investigating among others cyclone durations, propagation speeds, cyclogenesis, and -lysis regions. However, similar climatological studies regarding the life cycle characteristics of the cyclone's associated fronts are still missing. Previous work has either focused on individual model forecasts and case studies (Hewson 2009) or idealised model simulations (e.g., Dacre and Gray 2006). Numerous studies have been published on front climatologies (e.g., Jenkner et al. 2010; Berry et al. 2011; Catto et al. 2012; Rudeva and Simmonds 2015; Schemm et al. 2017), but these do not investigate the frontal life cycle, as fronts were only detected rather than also tracked over time. Simmonds et al. (2012) developed a front tracking method but used it only to discard short-living fronts from their analysis, and Rüdisühli (2018) used their front tracking algorithm mainly to identify mobile fronts and attribute frontal precipitation over time.

To be able to investigate life cycle characteristics of thousands of fronts, objective methods to detect and track these fronts have to be applied. While objective front detection methods have been widely used in climatological studies (e.g., Hewson 1998; Jenkner et al. 2010; Catto and Pfahl 2013; Schemm and Sprenger 2015; Schemm et al. 2017; Schaffer et al. 2024), tracking the identified front objects over time has rarely been attempted. Numerous tracking methods exist for cyclones, where a cyclone is identified as a single point in space (e.g., the minimum in the mean sea level pressure or relative vorticity field) and thus can be tracked following this point over time (Ulbrich et al. 2009; Neu et al. 2013; Dowdy and Catto 2017; Karwat et al. 2024).

Simmonds et al. (2012) adapted this approach for fronts, by first identifying a front as a collection of frontal points and then tracking the centre of gravity of these points by estimating the next position with the mean wind field. This circumnavigates the challenge of tracking each frontal point individually. However, since fronts are highly variable, the centre of gravity will fluctuate, and the track will appear rough. Rather than tracking a single or multiple individual points, Rüdisühli (2018) developed a method using two-dimensional front objects, which can be tracked over time by evaluating the overlap of these objects at consecutive time steps. This approach is better suited to deal with the highly variable shape and size of fronts, as it tracks the entire front object rather than a single point. Similar approaches have also been used to track cyclone objects (Wernli and Schwierz 2006; Hanley and Caballero 2012).

In this study, we detect and track cyclones and cold fronts in the ERA5 reanalysis data set over the North Atlantic and Europe. Cyclones and fronts are matched to create a data set of front-cyclone pairs. Results are used to investigate, for the first time, the climatology of frontal life cycle characteristics and their dependency on the North Atlantic Oscillation (NAO), the main mode of variability in this region (Hurrell et al. 2003), as well as relationships between fronts and their associated cyclones. We aim to address the following questions:

- Where, within our study region, do fronts typically form and where do they decay?
- How do the distributions of key characteristics of the frontal life cycle (strength, duration, travelled distance, speed, length) over the North Atlantic and Europe look
- How are these distributions influenced by the NAO?
- When and where in their life cycle do fronts reach their maximum intensity in terms of several frontal parameters?
- How strong are the relationships between frontal parameters and cyclone characteristics, and how do they change over time?

In Section 2, the used data as well as the methods for cyclone and front detection and tracking, the matching between cyclones and fronts, and the investigated frontal parameters and life cycle characteristics are presented. The results are outlined in Section 3 and discussed and summarised in Section 4.

2 | Data and Methods

2.1 | Data

For this study, we use the ERA5 reanalysis data set from the European Centre for Medium-Range Weather Forecasts (ECMWF) (Hersbach et al. 2020). The study region extends from 65W to 45E and 27N to 72N, which encompasses the North Atlantic, including its main region of frontogenesis, and large parts of Europe, including the Mediterranean (see Figure 1). We limited the analysis to the extended winter season (October–March), as the front tracking gets more challenging towards the summer months and a larger number of tracks become unreliable (see also in Section 4). All variables are extracted on a longitude-latitude grid with a resolution of 0.25° and for every hour in the period 1940–2021. The extracted variables are temperature, specific humidity, zonal wind speeds and geopotential height on 850 hPa, where the front detection and tracking is applied, as well as precipitation and surface wind components. Precipitation in ERA5 is the sum of large-scale precipitation and convective precipitation, which is generated by the cloud scheme and convection scheme of the ECMWF Integrated Forecast System (IFS), respectively. ERA5 precipitation has been evaluated in Lavers et al. (2022) against station data, where a small wet bias has been found, but with the smallest values in winter and in the extratropics.

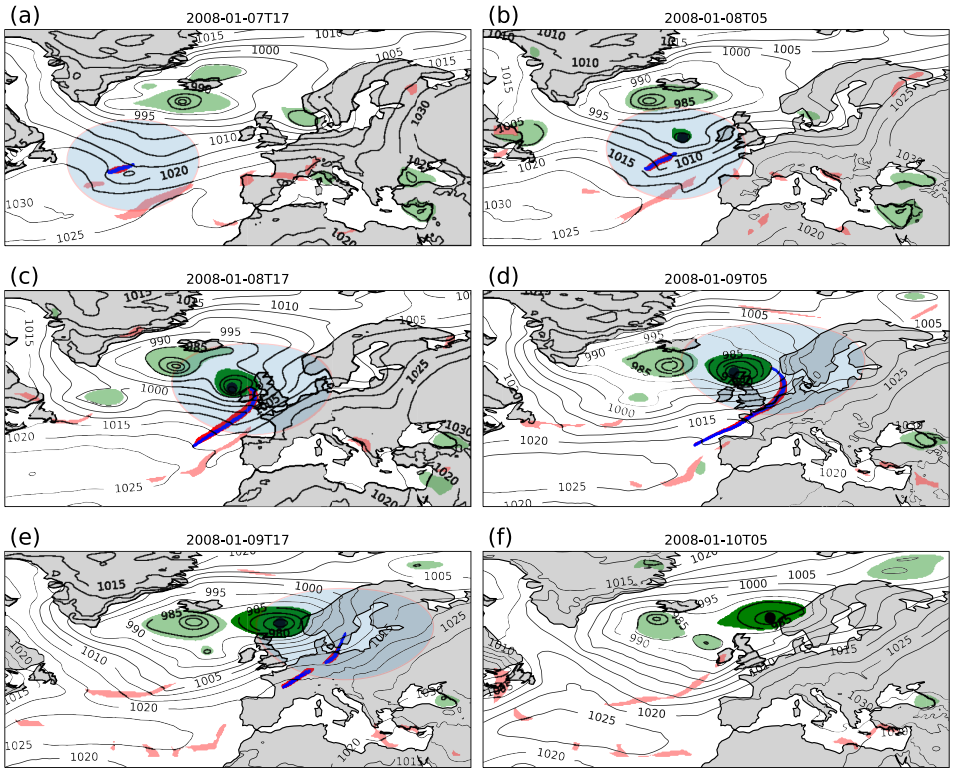

FIGURE 1 | An example of a cold front and cyclone track as well as the front—cyclone matching method. The SLP is shown as black contours. The red and green opaque areas show the tracked front and cyclone objects, respectively. More transparent areas depict other fronts and cyclones at the same time steps. For the featured track the detected frontal points are shown in blue. The light blue circle indicates the search region around the front for the cyclone-front matching. The plotted area indicates the study region. [Colour figure can be viewed at wileyonlinelibrary.com]

2.2 | Front Detection

To objectively detect fronts in a gridded data set, we use a similar method as in Schaffer et al. (2024). First, a threshold is applied to the magnitude of the gradient of a thermal field τ. This results in a set of distinct two-dimensional objects, i.e. contiguous regions where the threshold is exceeded. From here on, we refer to these objects as "front objects". Different τ have been used in the literature, including potential temperature θ (e.g., Renard and Clarke 1965), wet bulb potential temperature θ_w (e.g., Hewson 1998; Berry et al. 2011), equivalent potential temperature θ_e (e.g., Jenkner et al. 2010; Schemm et al. 2017; Rüdisühli 2018; Schaffer et al. 2024) as well as dynamic fields like the wind direction (Simmonds et al. 2012). Here, we use θ_e as our τ, as it also contains information of the humidity field and is conserved in moist adiabatic motions. This circumnavigates issues in detecting and tracking fronts in situations of e.g. strong differential heating between the cold and warm side of a front during daytime, where the temperature gradient might vanish for a few hours but the humidity gradient is still present and detected as a front (Lackmann 2011). The θ_e field is smoothed before calculating the gradients, by using a spectral filter and a low-pass filter, which preserves wavelengths larger than 1000 km and weights smaller wavelengths according to a spectral Gaussian transfer function with a mean of 1000 km and a standard deviation of 75 km. An example of relevant fields before and after applying these filters is shown in SI Figure S1. This results in more coherent fronts and filters out small-scale fronts, which are often found at land-sea boundaries or are related to orography. The choice of the threshold applied to the $\nabla\theta_e$ field is outlined in Section 2.3.

In a second step, the thermal front parameter TFP (Renard and Clarke 1965) is evaluated within the front objects:

$$\mathrm{TFP} = -\nabla\,|\,\nabla\theta_e\,| * \frac{\nabla\theta_e}{|\,\nabla\theta_e\,|} \tag{1}$$

which is the second derivative of the θ_e field, projected in the direction of its gradient. The actual front itself is then defined as the set of grid points (frontal points) within the front object where the TFP field reaches zero (Ritter 2014). These frontal points typically form a (bent) line.

Frontal points corresponding to a cold front are identified by evaluating the frontal motion v_f, which is defined as the projection of the horizontal wind field onto the direction perpendicular to the front, where the front direction is represented by the gradient of the TFP (e.g., Hewson 1998; Jenkner et al. 2010):

$$v_f = \boldsymbol{v} * \frac{\nabla(\mathrm{TFP})}{|\,\nabla(\mathrm{TFP})\,|} \tag{2}$$

Positive values correspond to cold fronts and negative values to warm fronts. We chose a threshold of 1.5 m/s to discriminate cold fronts from other front types and to keep only mobile fronts in the data set. Furthermore, individual frontal points are discarded, if the angle difference between the geopotential gradient and the direction of $\nabla\theta_e$ is exceeding 120°. This filter is found to effectively get rid of back-bend occlusions as well as humidity fronts which are detected, e.g., after a front passes over a large

mountain range. An example for applying this filter is shown is SI Figure S2.

2.3 | Front Tracking

To be able to follow fronts over time, a front tracking method is applied, based on an algorithm outlined in Rüdisühli (2018). This algorithm is based on the overlap of the 2-dimensional front objects, defined in Section 2.2, at consecutive time steps. By iterating through all time steps, for each object at the current time step, all objects at the next time step with a non-zero overlap are identified and vice versa. This creates a set of possible correspondences between an object at a certain time step (the parent) and one or more objects at either the previous or the next time step, representing either a possible continuation (one child), merging (two or more children at the previous time step) or splitting (two or more children at the next time step). For all possible correspondences a tracking probability p_t is calculated, based on the overlap ratio r_o and the size ratio r_s between the parent and the child or children:

$$p_t = \alpha * r_o + (1 - \alpha) * r_s \tag{3}$$

where α is a weighting factor. By going through the list of descending probabilities, all objects are then assigned to their most likely correspondences. The remaining objects mark then either the beginning of a new track (at the next time step) or the end of a track (at the previous time step). In case of a split or merge, only the track with the highest p_t will be preserved. All other branches will either end (merge) or start new tracks (split), except for branches which have developed over the last 12 h or are decaying in the next 12 h, in which case they will be added to the main track. The chosen values for the parameters (SI Table S1) are similar as in Rüdisühli (2018), except for a lowered minimum size ratio, which is found to better capture front continuations in cases of splitting or merging and a higher minimum object size to remove small front objects.

The $\nabla\theta_e$ threshold used to identify the objects was chosen such that the resulting objects are broad enough to have sufficient overlap at consecutive time steps even for fast moving fronts, but also not overlap with neighbouring fronts at the same time. The threshold is slightly varying over the domain and over the yearly cycle, taking into account the differences in the $\nabla\theta_e$ field near fronts in different regions (higher values over the Atlantic, lower values over land) and different seasons (lower values in winter, higher values towards summer). Applying a constant threshold over space and time would lead to very broad objects over the Atlantic and in summer, so that fronts close to each other would be identified as one object and therefore one contiguous front, and too small or even no objects and therefore tracks over the continent and in winter. The finally chosen threshold is proportional to the $\nabla\theta_e$ field, averaged over the study period 1940–2021 (SI Figure S3).

After tracking the front objects, all front pixels obtained from the front detection, which lie within the tracked objects by construction, are labelled according to the objects. In order to capture only fronts that experience their full life cycle within the domain, front tracks with front pixels touching the domain border at their first (last) detected time step are assumed to have started (have ended) their life cycle outside the domain and are therefore discarded. Additionally, as the tracking algorithm only preserves the track with the highest tracking probability in cases of splitting or merging, tracks that start in a splitting event or end in a merging event are also filtered out, as these tracks will most likely not represent a full frontal life cycle.

2.4 | Cyclone Detection and Tracking

To detect cyclones, we use the same algorithm as Rüdisühli (2018), which is based on a method developed by Wernli and Schwierz (2006) and Hanley and Caballero (2012). First, SLP minima are identified as grid points with lower values compared to their eight neighbouring grid points. Points within three grid points from the domain boundary as well as points corresponding to a topographic height of over 1500 m are ignored to avoid artefacts and misidentifying lows as cyclones over high topography. Next, by subsequently checking the contour lines with an interval of 0.5 hPa around the minima, the outermost enclosing contour lines are found, defining the cyclone objects. To avoid restricting the size of cyclones close to the boundaries of our domain by this method, a fraction of 20% of all contour lines around a minimum are allowed to leave the domain (Rüdisühli 2018). The cyclone objects are checked for a sufficient depth, i.e. the pressure difference between the cyclone centre and the outermost contour line of the cyclone object, where we use a threshold of 0.5 hPa to capture new developing cyclones as early as possible while avoiding misidentifying e.g. shallow heat lows over land as cyclones. Heat lows that might exceed the minimum depth threshold are further filtered by applying a minimum object size and track length threshold. Following Hanley and Caballero (2012), we split objects with multiple minima into multiple objects if the depth of the saddle point between two minima divided by the total depth of the object exceeds 50% (objects with two minima) or 70% (objects with three minima).

The cyclone tracking is then performed in a similar fashion as the front tracking, where the identified cyclone objects act as the objects to track (see SI Table S2 for the cyclone tracking setup).

2.5 | Front-Cyclone Matching

To be able to investigate cyclone-front relationships, it is necessary to identify the cyclone to which a front is attached. Schemm et al. (2018) used the same cyclone detection method and attributed at each time step the detected fronts which overlap with the cyclone mask to the cyclone. However, there are frequent cases where e.g., cyclones form in the vicinity of a primary cyclone, usually along the trailing cold front (Parker 1998; Schemm and Sprenger 2015; Schemm et al. 2018; Priestley et al. 2020). These cyclones are called secondary cyclones and their cyclone mask in the detection scheme is usually small at the beginning of the track as it is dominated by the primary cyclone. This, however, will often lead to no overlap between the cyclone mask and the detected front. Therefore, instead of considering the overlap of the cyclone mask and the detected front, we search for cyclone centres in a radius of 1200 km around the frontal point which is

assumed to be closest to the cyclone centre. This search point is defined as the northernmost (easternmost) detected frontal point if the main orientation of the front is north–south (west–east). If there are multiple cyclone centres found within the radius, the closer cyclone is chosen and labelled as the associated cyclone of the front. We chose a rather large value of 1200 km for the search radius, as we found it to be beneficial in rare cases where the cold front is detected only late in its life cycle because of a weak $\nabla\theta_e$ in the beginning and therefore might be already detached from the cyclone centre due to frontal fraction. This procedure is then repeated over all time steps of the front track. In the end, only those front tracks which are associated with the same cyclone over at least 12 h and 50% of their life time are kept in the data set.

Figure 1 gives snapshots over the life cycle of a front for an event in January 2008, depicting the tracked front and cyclone objects, the detected frontal points, and the search radius of the cyclone-front matching method. First, a cold front forms over the central North Atlantic in a trough of a larger cyclone system over Iceland (Figure 1a). The associated secondary cyclone developing along the front is detected a few hours later and is matched with the front, as its cyclone centre lies within the search radius of the front (Figure 1b). The cyclone-front system then moves further northwest over the British Isles while intensifying (Figure 1c,d). The front eventually gets weaker and splits up when moving into Central Europe (Figure 1e) and finally decays (Figure 1f), while the cyclone remains relatively stationary off the Norwegian coast.

2.6 | Diagnostics and Frontal Parameters

In order to characterise the frontal life cycle, we investigate the duration of the track, the overall travelled distance of the front, the frontogenesis and -lysis point, as well as the velocity and the length of the front. Some of these measures are evaluated for the centre of mass (CM) of the frontal points, whose latitude and longitude are defined as

$$\varphi_{\mathrm{CM}} = \frac{1}{N}\sum_{i=1}^{N}\varphi_i \quad \text{and} \quad \lambda_{\mathrm{CM}} = \frac{1}{N}\frac{\sum_{i=1}^{N}\lambda_i\cos(\varphi_i)}{\sum_{i=1}^{N}\cos(\varphi_i)} \tag{4}$$

where φ_i and λ_i are the latitudes and longitudes of the individual frontal points. The frontogenesis (frontolysis) point is then simply the CM of the first (last) time step of the track. The velocity of the object at time step t is defined as

$$v_t = \left(X_{t+1} - X_{t-1}\right)/2\Delta t \tag{5}$$

where X_{t+1} and X_{t-1} are the positions of the CM at the next and previous time step and Δt the time difference between consecutive time steps. The velocity is not evaluated at time steps where there is a merging or splitting, as this would lead to unrealistic values with this method, due to the sudden change of the objects shape. The overall travelled distance is the sum over the distances between consecutive time steps:

$$D = \sum_{t=1}^{N}\left(X_{t+1} - X_t\right) \tag{6}$$

The spatial length of a front at each time step is approximated by evaluating the diagonal of the smallest rectangle encompassing all contiguous frontal points. If the front consists of multiple separated parts, the obtained lengths of each part are added together. A more accurate way to estimate the front length would be to calculate and sum up the distances between neighbouring individual frontal points, which would better account for strongly bended fronts (Simmonds et al. 2012). By comparing estimated lengths from both methods using a sub-sample of our data, We find the number of cases where this leads to significant differences to be small; thus, we choose the computationally more efficient method.

To characterise the dynamical and thermodynamical state of the front as well as the surface impacts, the 90th percentile of several parameters are evaluated in a radius of 150 km around each frontal point and at the same level (850 hPa) where the fronts are detected (Schaffer et al. 2024). Those include precipitation and surface wind speeds to assess the surface impacts, thermodynamic parameters (specific humidity, θ and θ_e as well as their gradient) and dynamic parameters (vorticity, convergence and cross-front wind speeds). Wind speeds are further evaluated in the warm (cold) sector of the front separately, defined as the grid points within the 150 km radius, where the TFP is above the 90th percentile (below the 10th percentile). Additionally, the wind speed is split into the synoptic- and meso-scale by using the same spectral filter as in the front detection, with the high pass of the Gaussian Transfer Function set to 1500 km with a standard deviation of 500 km. To characterise the parent cyclone of a front, we use sea level pressure (SLP) and vorticity as well as the deepening rate (in hPa/h) of the cyclone centre.

To analyse relationships between cyclones and their associated fronts, we use a quantile regression model (Koenker 2005), with cyclonic parameters acting as predictors and frontal parameters acting as predictands. The conditional 50th, 80th, and 95th percentiles as well as the respective Quantile Verification Skill Score (QVSS) are estimated to depict changes in the relationships and to quantify the explained variance (Koenker and Machado 1999; Friederichs 2010). The relationships are evaluated at different times relative to the maximum cyclone strength (measured as minimum central pressure and maximum relative vorticity) and maximum cyclone deepening (measured as change of minimum central pressure over time) to assess changes over time.

3 | Results

3.1 | Life Cycle Characteristics

The number of cold frontogenesis and frontolysis occurrences are shown in Figure 2. The location of frontogenesis and -lysis is defined as the CM of frontal points at the first and last tracked time step of each front. Cold fronts are found to form primarily along the North Atlantic storm track region (Figure 2a), with highest values south-east of the coast of Newfoundland, a region known also for frequent cyclogenesis (Dacre and Gray 2009; Gramcianinov et al. 2020). Other regions of enhanced frontogenesis are found near the southern tip of Greenland and over the Western and Central Mediterranean, related to Genoa lows. The enhanced values over the Southern British Isles are partly

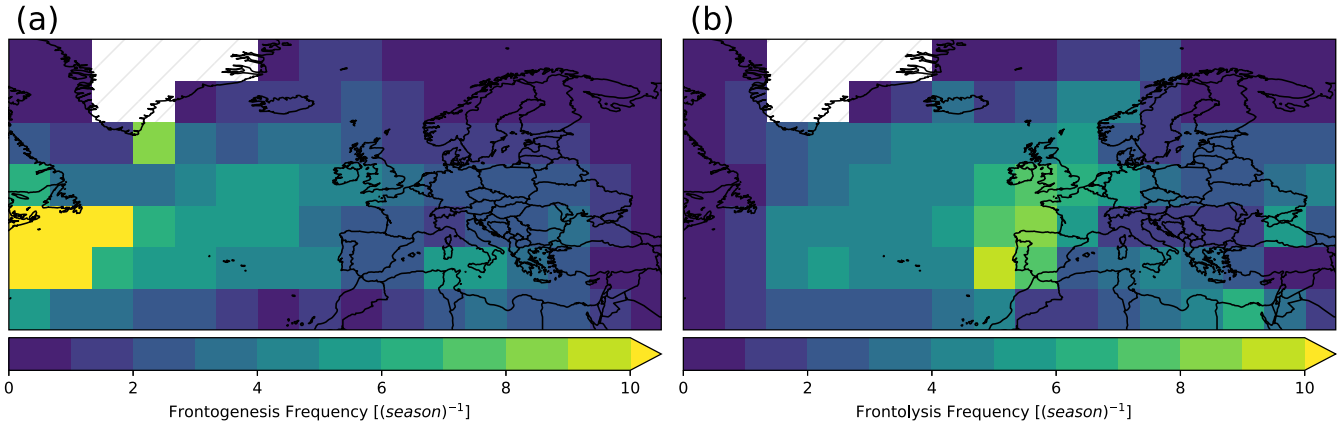

FIGURE 2 | (a) Cold frontogenesis and (b) frontolysis occurences for the extended winter season (October–March) of the years 1940–2022. Hatched areas indicate grid points excluded from the analysis (mean elevation > 1000 m). [Colour figure can be viewed at wileyonlinelibrary.com]

caused by fronts moving in from the North Atlantic and falling under the $\nabla\theta_e$ threshold for a few hours before strengthening again, so that they were recognised as a newly developing front by the algorithm rather than the continuation of the old track.

Most fronts forming in the North Atlantic are found to decay when they reach the European coast (Figure 2b). While this can be explained by the dissipation of $\nabla\theta_e$ due to friction over Land and—to a lesser extend—the diurnal land-sea thermal gradient, the ratio of fronts continuing over the continent is likely to be underestimated. This is due to splitting and decaying fronts along mountain ranges like the Alps or Scandinavian Mountains, which block fronts at lower levels and might end the track prematurely. The maximum frontolysis off the Portuguese coast stems partly from fronts splitting into two parts when approaching the coast of Galicia. Especially for long fronts, the algorithm most likely evaluates the southern part as the continuation of the track, since it is often longer and moving slower than the northern part and therefore exhibits higher values for r_o and r_s (see Equation 3). Other regions of enhanced frontolysis are found over the Eastern Mediterranean, which are mostly fronts associated with Mediterranean cyclones forming over the Western and Central Mediterranean and moving eastward, and near the Black Sea.

Figure 3 depicts the spatial distribution of the life cycle characteristics, where every grid point shows the mean over all fronts passing through this grid point. With this representation, the same front track will be represented in multiple grid points as the front moves through the domain, resulting in smooth out values and a slight overrepresentation of long lasting or farther travelling tracks. Values for $\nabla\theta_e$ (Figure 3a) are highest over the Western and Central North Atlantic off the coast of Newfoundland, consistent with the region of most frequent frontogenesis (Figure 2). The values get weaker towards and especially over the continent, which is caused by the dissipation of $\nabla\theta_e$ due to increased friction over the continent. Slightly higher values can also be seen over the Mediterranean, another region of enhanced frontogenesis. Fronts generally live longer and travel farther over the Ocean than over Land (Figure 3b,c). While the average duration over the Central North Atlantic reaches 2–2.5 days, it drops to 1–2 days for fronts over the Eastern Mediterranean, Eastern Europe and the Greenland Sea. Fronts over the Mediterranean are generally shorter in duration and distance since less North Atlantic fronts penetrate into these regions than more northern parts of Europe. Values towards the eastern and northern boundary of the domain could be affected by not considering tracks which leave the domain during their life cycle. Fronts over the Labrador Sea often stay stationary and are short-lived, which is reflected in low durations, travelled distances and velocities. The highest travelled distances are found over the Central North Atlantic and at the western border of the domain, since most fronts originating there are found to travel over the North Atlantic towards Europe and decay quickly when they pass over Land. The values of around 3000 km therefore correspond roughly to the distance to the European coast. Fronts are found to reach their maximum length and velocity over the Central North Atlantic, with mean values of up to 1200 km and 70 km/h (Figure 3d,e). Velocities are considerably lower towards the boundaries of the domain, suggesting that fronts are generally faster during the mature stage of their life cycle rather than towards frontogenesis or -lysis. Fronts over the Western North Atlantic obtain a mean length of up to 1500 km, dropping towards the Eastern North Atlantic and Europe. This suggests that fronts forming in the main frontogenesis region in the Western North Atlantic quickly grow in length in the beginning of their life cycle and then are shortened slowly while moving eastward (see SI Figure S4 for a length comparison of fronts forming over the Western North Atlantic and elsewhere). Over the Mediterranean, fronts generally travel shorter distances and move slower, with mean values of 700–900 km and 40–50 km/h, respectively.

Figure 4 shows the location and magnitude of the life cycle maximum of some frontal parameters. Blue circles indicate the number of fronts reaching the life cycle maximum of the respective frontal parameter within the grid box (the front location is defined as the CM of all frontal points at the time step of the life cycle maximum) and the colour map indicates the mean magnitude of all fronts with life cycle maxima within the grid box.

Most fronts reach their maximum speed over the Central North Atlantic or before arriving at the European coast (Figure 4a). Enhanced values seen in e.g. Southern Norway, Northern Italy and around the Black Sea are affected by unrealistically high frontal speeds in cases of splits, where the CM suddenly changes

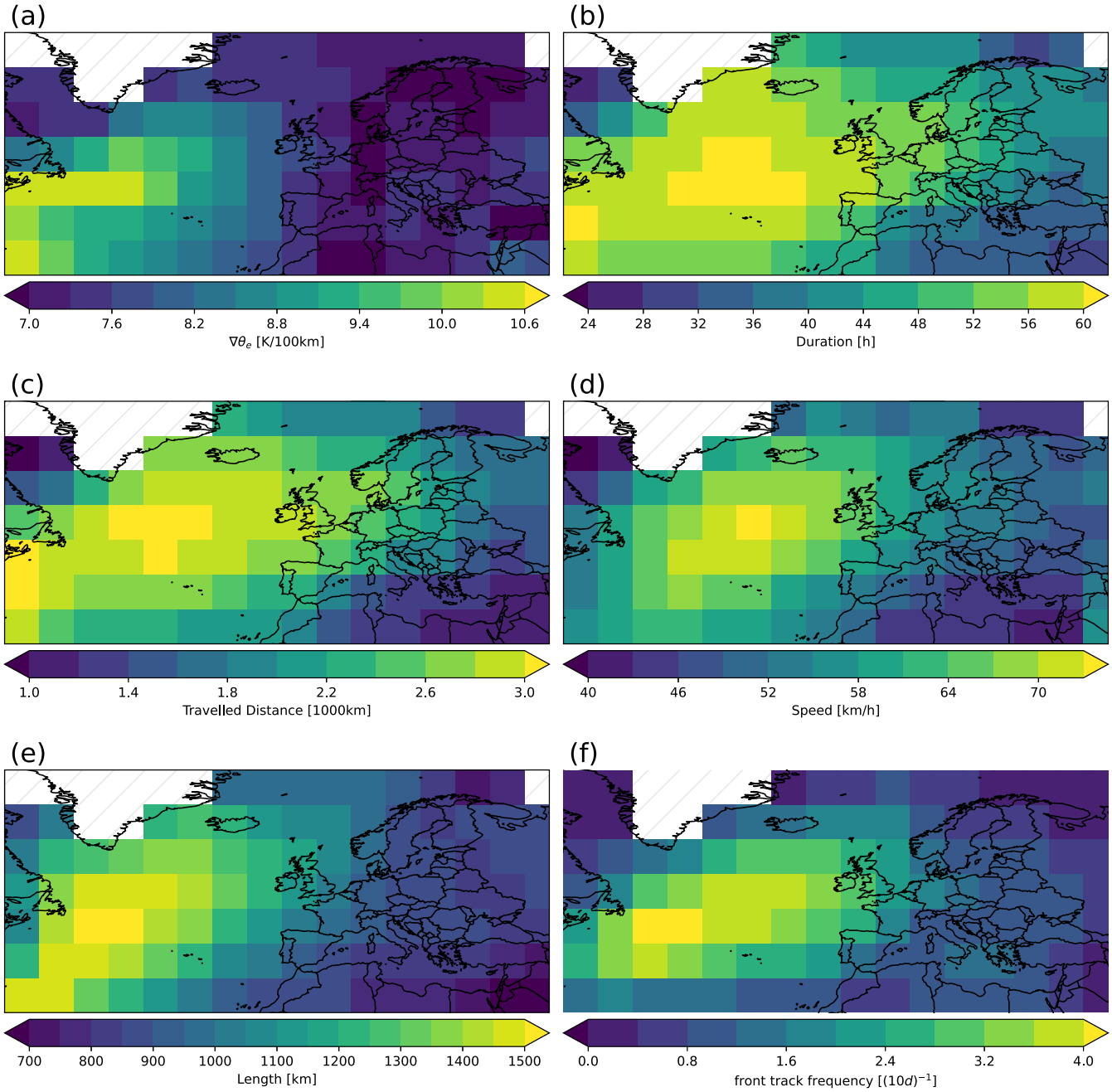

FIGURE 3 | Spatial maps of cold frontal life cycle characteristics for the extended winter season (October–March) of the years 1940–2022: (a) thermal gradient field, (b) front duration, (c) total travelled distance, (d) front speed, (e) front length, (f) front frequency. Each grid box represents the mean over all fronts passing through the grid box. Hatched areas indicate grid points excluded from the analysis (mean elevation > 1000 m) or where there is a too small sample (less than 50 fronts, for (a)–(e)). [Colour figure can be viewed at wileyonlinelibrary.com]

location. While we tried to filter these cases by taking into account the simultaneous change in front length, not all cases could be avoided. Fronts reach their maximum length generally earlier in their life cycle than their maximum speed, as the highest frequencies and values are shifted towards the Western North Atlantic (Figure 4b). A pronounced maximum area is found from 55W to 30W and 35N to 55N. Note that values near the boundary are underestimated since they are plotted at the CM of the front and therefore only very short fronts contribute to the outermost grid boxes. Most fronts are strongest in terms of $\nabla\theta_e$ close to the regions of highest frontogenesis (Figure 4c), suggesting that fronts in general reach their maximum strength very early in their life cycle and then decaying slowly. Maximum values are generally much higher for fronts over the North Atlantic than over the continent and the Mediterranean. In Figure 4d, the location of the maxima of the frontogenesis parameter (Bluestein 1992), which quantifies the horizontal dynamical effects on changes of $\nabla\theta_e$, also correlates with regions of high frontogenesis (Figure 2a). Highest magnitudes are found over the western North Atlantic and also over the Mediterranean, indicating frontal activity and strong dynamical growth of fronts developing there. The maximum wind speeds in the cold and warm sector of the front at 850 hPa (Figure 4e,f) are found all along the North Atlantic storm track, with maximum values

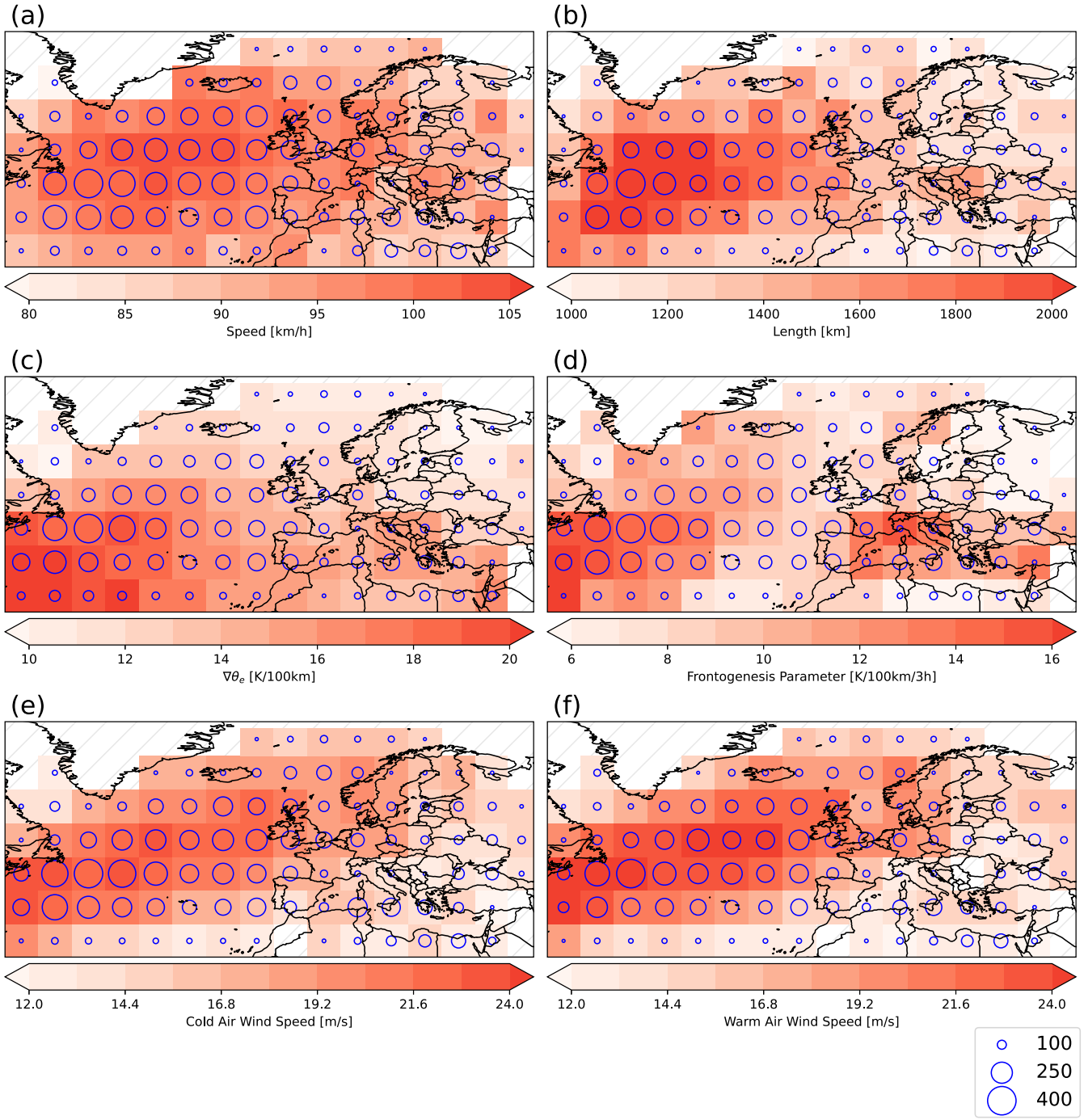

FIGURE 4 | Frequency and magnitude of cold frontal life cycle maxima for some frontal parameters and diagnostics for the extended winter season (October–March) of the years 1940–2022. Blue circles indicate the total number of tracked fronts in the period 1940–2022 with their life cycle maxima location falling within the grid box. The colour map shows the mean magnitude over all life cycle maxima falling within the grid box. The location of a front is defined as the CM of all individual frontal points. Hatched areas indicate grid points excluded from the analysis (mean elevation > 1000 m) or where there is a too small sample (less than 50 fronts). [Colour figure can be viewed at wileyonlinelibrary.com]

reaching 25 m/s, where wind speeds in the warm sector (which can be seen as a proxy for the wind speed in the warm conveyor belt inflow) are found to be higher on average.

3.2 | NAO Dependency

Figure 5 shows histograms of life cycle characteristics obtained from all fronts in the data set for the entire domain. Fronts are divided into fronts occurring in a NAO positive (NAO+) phase and a NAO negative (NAO−) phase, depending on the respective NAO index during the life cycle. Daily NAO index values were retrieved from the National Oceanic and Atmospheric Administration (https://www.cpc.ncep.noaa.gov/), where the index is calculated using Rotated Principal Component Analysis (Barnston and Livezey 1987), applied to 500 hPa geopotential height anomalies of the Climate Data Assimilation System (CDAS). Fronts are labelled as NAO+ (NAO−), if the mean

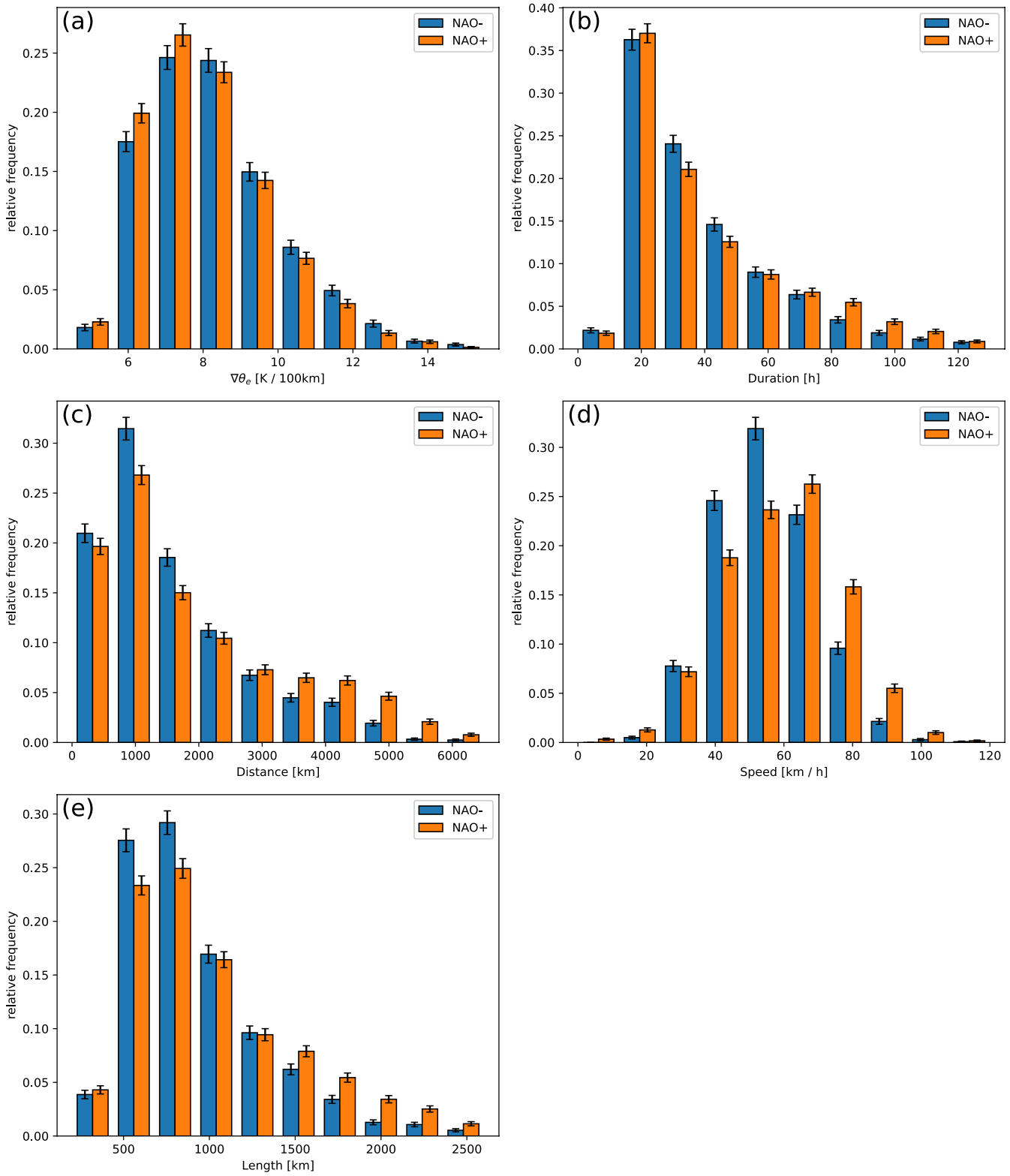

FIGURE 5 | Histograms of life cycle characteristics for cold fronts in a NAO+ and NAO− regime, respectively: (a) $\nabla\theta_e$, (b) life cycle duration, (c) travelled distance, (d) front speed and (e) front length. In (a), (d) and (e) mean values over all time steps of the life cycle are shown. The error bars represent the 95% confidence interval of each frequency value measured as $2 * \sqrt{N}$ with bin count N, assuming a Poisson distribution. [Colour figure can be viewed at wileyonlinelibrary.com]

daily NAO index on the days where the front occurs is above 0.5 (below −0.5). The front strength in terms of $\nabla\theta_e$ (Figure 5a), front speed and front length (Figure 5d,e) are mean values over the entire life cycle for an individual front.

For the mean front strength (Figure 5a), no significant differences between fronts in a NAO+ and a NAO− phase are found. Fronts in a NAO+ phase do, however, last longer and travel farther on average (Figure 5b,c). While in a NAO− phase about

10% of all fronts travel farther than 2500 km, this ratio doubles for fronts in a NAO+ phase. Front speeds differ by a mean of 11 km/h (from a mean speed of 51 km/h for fronts in a NAO− phase to 62 km/h for fronts in a NAO+ phase) (Figure 5d). Especially long fronts with lengths over 1200 km are more frequent in a NAO+ phase (Figure 5e).

Figure 6 depicts the spatial differences of life cycle characteristics between fronts in a NAO+ and NAO− phase. The differences in front strength (Figure 6a) are weak, with fronts in a NAO− phase found to be slightly stronger except for the Central Southern North Atlantic, which might be linked to the equatorward displacement of the storm track and the jet stream in a NAO− phase. Fronts in a NAO+ phase exhibit longer durations over Central and Northern Europe and, to a lesser extent, over the Atlantic and shorter durations over the Mediterranean (Figure 6b). Similar patterns can be seen for the travelled distance, mean frontal speed, and frontal length (Figure 6c–e), with particularly high differences in distance for fronts over Northern Europe and in length for fronts around Iceland. Changes in frontal frequencies (Figure 6f) in different NAO phases show a dipole structure, with enhanced activity over the northern North Atlantic and Northern Europe and reduced activity over the southern North Atlantic, the Mediterranean, and Eastern Europe. This is in agreement with previous studies (Rudeva and Simmonds 2015) and correlates strongly with changes found for cyclone activity depending on the NAO phase (Rogers 1997; Pinto et al. 2009; Rudeva and Simmonds 2015).

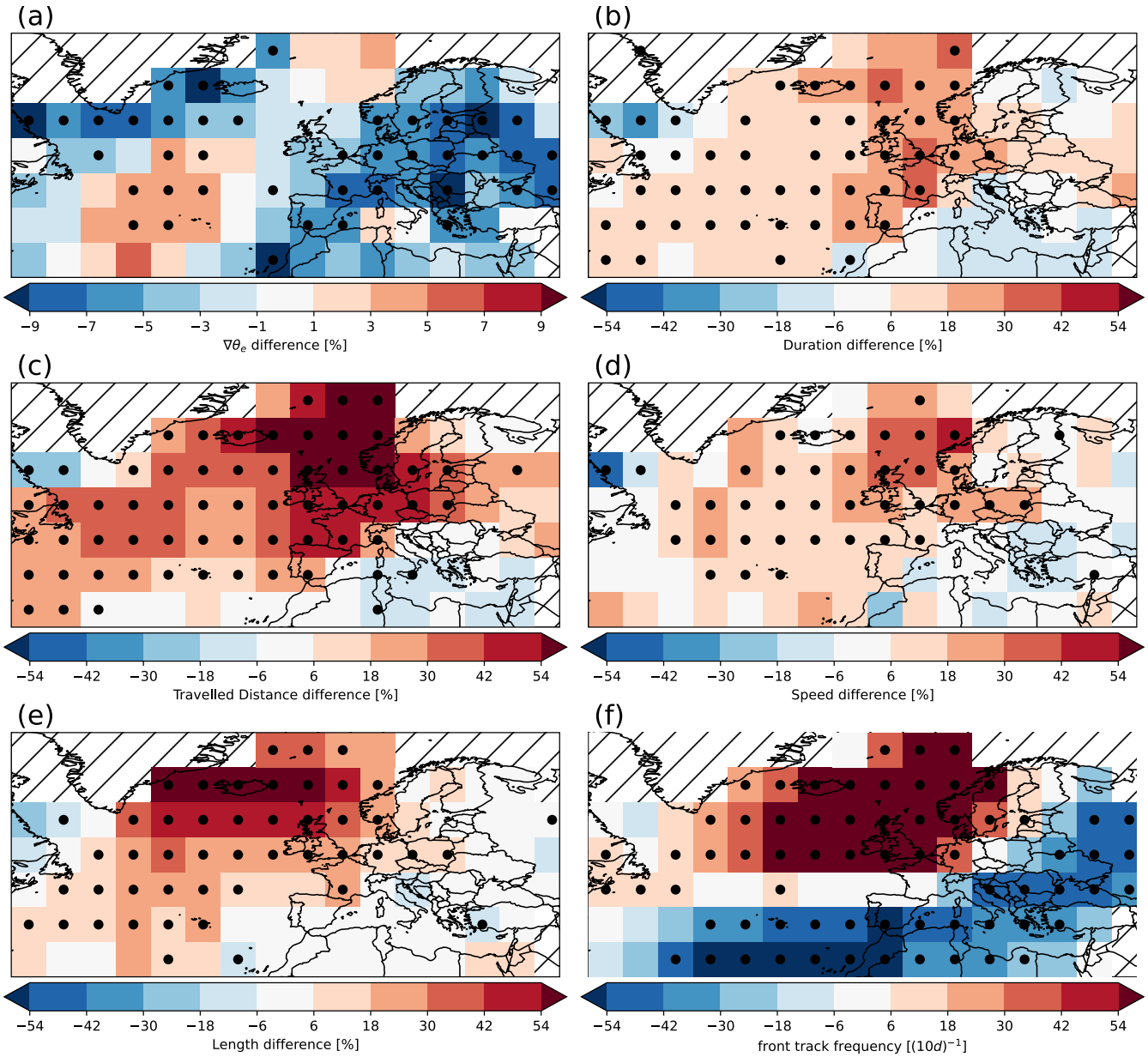

FIGURE 6 | As Figure 3, but for cold fronts appearing in a NAO+ phase subtracted by cold fronts appearing in a NAO− phase. Note the different colour map scale of (a) compared to (b)-(f). Dots mark grid boxes where the difference is significant based on a two-sample Kolmogorov–Smirnov (a–e) and χ^2 (f) test and 95% confidence level. Hatched areas indicate grid points excluded from the analysis (mean elevation > 1000 m) or where there is a too small sample (less than 50 fronts). [Colour figure can be viewed at wileyonlinelibrary.com]

These patterns can be explained by the overall stronger westerly flow and the extended storm track over the North Atlantic and Northern Europe in a NAO+ phase (Rogers 1997; Hurrell and Deser 2010; Feser et al. 2015) due to a stronger jet stream and enhanced baroclinicity (Pinto et al. 2009), which is also linked to upper-tropospheric frontogenesis (Davies and Rossa 1998).

3.3 | Front-Cyclone Relationships

In Figure 7 the relationships between selected frontal parameters and the cyclone centre SLP are shown. Points are plotted at the time step of minimum cyclone SLP for each front-cyclone pair. A linear quantile regression model is fitted to the data, and the 50th, 80th, and 95th percentile lines, as well as their 95% confidence interval, are plotted. The QVSSs for all quantiles and all frontal parameters, as well as scatter plots for cyclone vorticity and cyclone deepening, are depicted in SI Figures S5 and S6 and Tables S3 and S5.

The cyclone SLP has the highest correlations with dynamic frontal parameters, with QVSS ranging from 17% to 20% (15% to 17%) for the total wind speeds in the warm (cold) sector of the front, 13%–17% for the cross-front wind speed and 16% for the

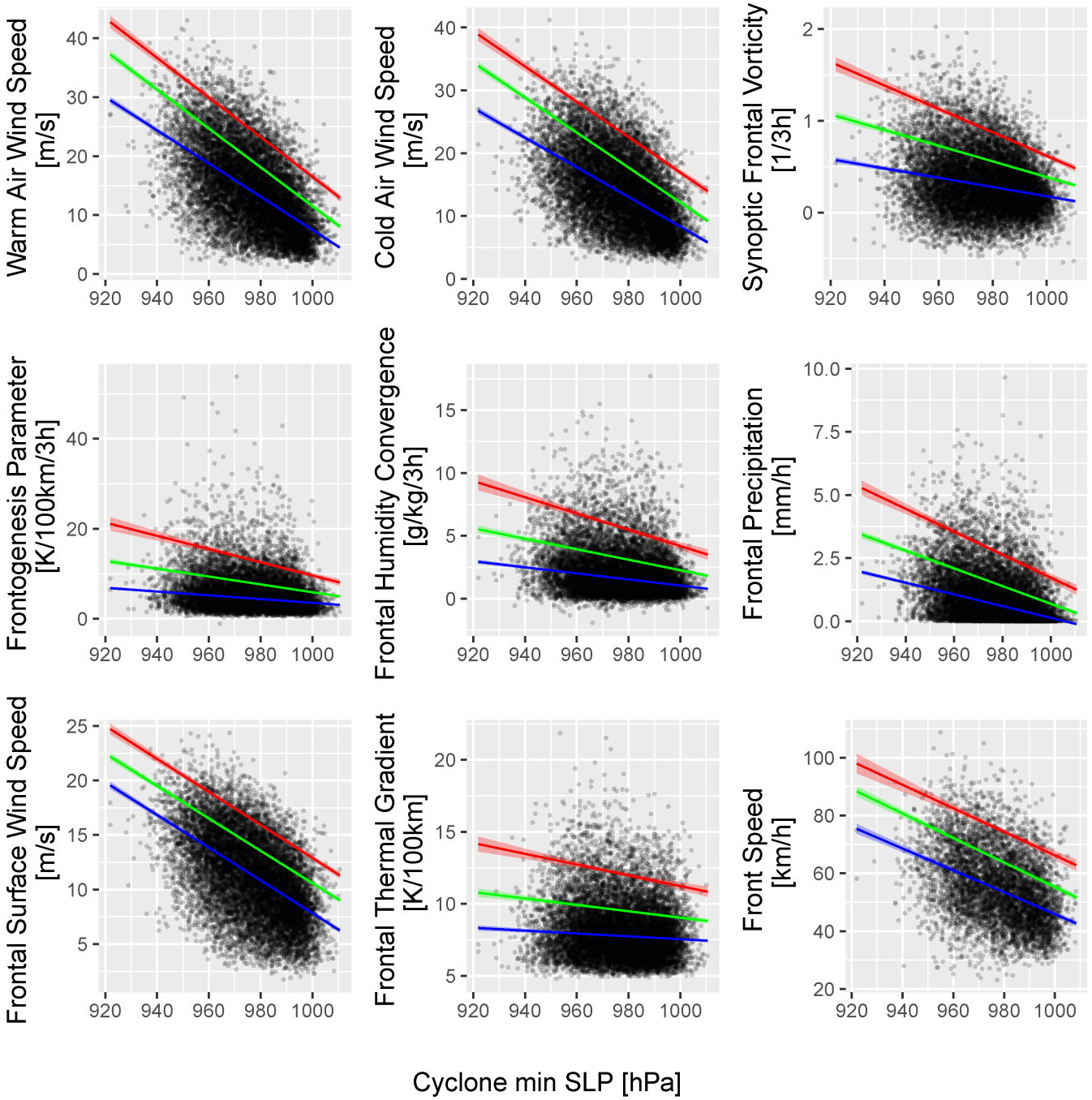

FIGURE 7 | Relationships between frontal parameters and the cyclone SLP at the time step of maximum cyclone intensity. Points indicate individual front-cyclone pairs and lines indicate the 50th (blue), 80th (green) and 95th (red) percentile obtained from quantile regression. Shaded areas depict the 95% confidence interval obtained from bootstrapping. [Colour figure can be viewed at wileyonlinelibrary.com]

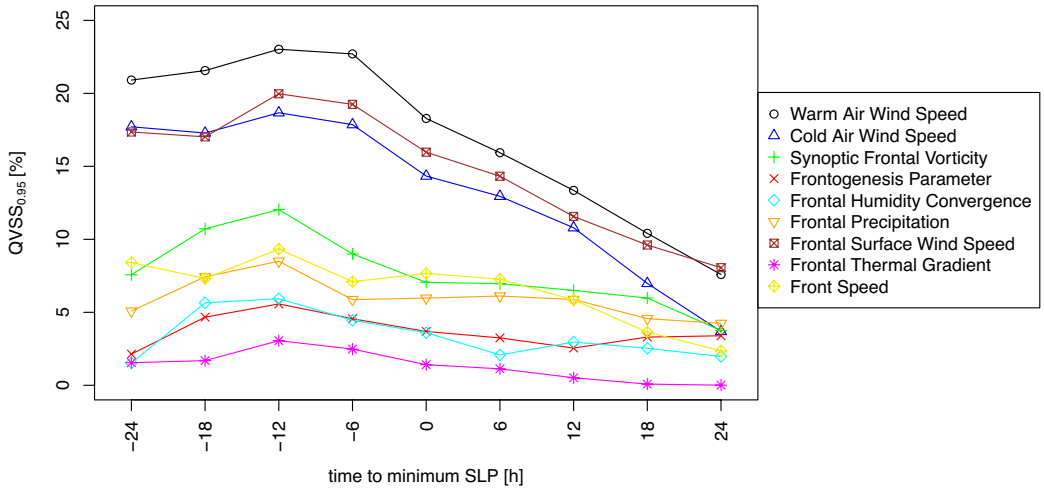

FIGURE 8 | Quantile Verification Skill Scores of the quantile regression between the cyclone SLP and frontal parameters for different times relative to the minimum cyclone SLP. Only values for the 95th percentile are shown. [Colour figure can be viewed at wileyonlinelibrary.com]

frontal surface wind speeds. This is in agreement with previous studies outlining the importance of the cyclone intensity for low-level and surface wind speeds (Roberts et al. 2014; Hewson and Neu 2015; Owen et al. 2021). The QVSS for frontal vorticity shows a large spread between different quantiles (5%–16%), indicating a non-linear relationship. The cyclone SLP shows medium predictive power of 5%–8% for frontal precipitation. Field and Wood (2007) have shown a stronger correlation between mean precipitation values in a 2000 km radius around the cyclone centre and the cyclone strength (in terms of mean surface wind speeds in a 2000 km radius around the cyclone centre), indicating that processes on smaller scales along the front play a more dominant role in shaping frontal precipitation. Stronger cyclones are also moderately associated with faster moving fronts. The correlation with gradients of thermodynamic frontal parameters such as frontal strength (measured as $\nabla\theta_e$) and humidity convergence is found to be weak. This can be partly explained by the dominant influence of local geographic factors, e.g. orography, on these parameters in Europe and the Mediterranean.

In Figure 8 the evolution of the 95th percentile QVSS over time relative to the time of minimum cyclone SLP is shown for several frontal parameters. While more thermodynamic parameters like frontal precipitation, humidity convergence and $\nabla\theta_e$ as well as the front speed have low to medium QVSS at all time steps, peaking 12 h before the cyclone reaches its minimum SLP and slowly decreasing afterwards, dynamic frontal parameters as the wind speeds in the cold and warm sector of the front, the cross-front wind speed and the frontal surface wind speed have a consistently high QVSS between 17% and 23% in the 24 h prior to maximum cyclone intensity, but drop rapidly afterwards. This might be attributed to the increasing distance between the cold front and the associated cyclone over their life cycle (SI Figure S7), weakening the relationships. This detachment has been already investigated by Schemm et al. (2018), who defined a cyclone to be attended by a front if the detected front overlaps with the 2D cyclone mask and found that the frequency of cyclones attended by a front drops from 80% to 40% over the course of their life cycle.

4 | Discussion and Conclusion

In this study, we analyse the life cycle of cyclone-associated cold fronts as well as front-cyclone relationships and for the first time, produced a climatology of life cycle characteristics over the North Atlantic and Europe. Front and cyclone detection and tracking methods are applied to the ERA5 reanalysis data set. Cold fronts are found to develop primarily over the Western North Atlantic in a region also known for enhanced cyclogenesis (Dacre and Gray 2009; Gramcianinov et al. 2020) and to often decay when they reach coastal areas of the European continent. Cold fronts following the North Atlantic storm track have on average a longer duration (50–65 h), a longer extent (1000–1500 km) and move faster (55–75 km/h) than fronts tracked over the Mediterranean and the European continent (average values 30–45 h, 700–1000 km, 45–55 km/h). The life cycle characteristics depend strongly on the NAO phase, with frontal activity increasing over the northern North Atlantic and Northern Europe in a NAO+ phase and decreasing over the southern North Atlantic, the Mediterranean and Eastern Europe in a NAO− phase. Rudeva and Simmonds (2015) found a similar dipole structure for the correlation of front frequency with the NAO phase, but with positive values also over Eastern Europe, in contrast to our findings. This might be due to a larger number of fronts in this region continuing to travel outside of our study domain—and therefore not being considered—in a NAO+ phase because of a more zonal and farther extending stormtrack. Furthermore, fronts are found to live longer, travel farther and faster and have a longer spatial extent over the North Atlantic and Western Europe in a NAO+ phase. We find cold fronts appearing in a NAO+ phase to be weaker by up to 10% in terms of their mean $\nabla\theta_e$ compared to cold fronts in a NAO− phase. We find wind speeds in the warm and cold sector of the cold front as well as on the surface to be strongly correlated with the intensity of the associated cyclone. The relationships between frontal and cyclonic properties are weakening over the course of their life cycle, possibly due to the cold frontal fracture.

Applying an objective front tracking algorithm over large domains and long periods is a challenging task as fronts are highly variable objects in space and time. The algorithm used in this

paper was chosen because it is based on a simple concept (overlapping objects), has been specifically designed to study fronts (Rüdisühli 2018) and is computationally efficient enough to apply it to a large data set. Other methods based, e.g., on a Lagrangian approach, might be in theory more suitable to capture the three-dimensional behaviour of a front over time, but would require more computational resources. In light of the computational resources and since multiple parameters have to be tuned not only for the front tracking but also for the cyclone tracking, the front and cyclone detection, and the front–cyclone matching to obtain the most reliable results possible, we chose to restrict our study region to the North Atlantic and the European continent, rather than to the whole Northern Hemisphere or even the entire globe.

Especially when moving over large mountain ranges (e.g., Alps, Pyrenees, Scandinavian Mountains, Dinaric Alps), front tracking becomes difficult, as fronts often vanish or disappear for some time before reappearing at the rear side of the mountain range. Therefore, the front tracks might end prematurely or start new tracks on the rear side, even if they are objectively the same front. This effect leads to a reduction in frontal frequency and the certainty of the front characteristics, especially in the Mediterranean. This issue could be circumnavigated by tracking and detecting fronts at higher levels (e.g., 700 hPa, Jenkner et al. (2010)). However, this would complicate the assignment of surface impacts to frontal points, as cold fronts usually slope backward with height.

The methodology applied in this paper might be used in further studies to evaluate climate models and their ability to represent fronts correctly, as well as to investigate the impact of climate change on fronts, their life cycle characteristics, and relationships with cyclones in climate model projections.

Author Contributions

Tobias Lichtenegger: conceptualization, investigation, writing – original draft, writing – review and editing, visualization, validation, methodology, software, formal analysis, data curation. **Armin Schaffer:** conceptualization, investigation, methodology, validation, software, formal analysis, data curation, writing – review and editing. **Albert Ossó:** conceptualization, formal analysis, supervision, writing – review and editing. **Oscar Martínez-Alvarado:** conceptualization, formal analysis, writing – review and editing. **Douglas Maraun:** supervision, project administration, conceptualization, methodology, funding acquisition, writing – review and editing.

Acknowledgements

This research was funded by the Austrian Science Fund (FWF) in the course of the INTERACT Project (Interactions across scales shaping frontal weather extremes in a changing climate) (I 4831-N). We further want to thank our scientific advisory board members, Stephan Pfahl and Laurent Terray, for supporting our research.

Conflicts of Interest

The authors declare no conflicts of interest.

Data Availability Statement

ERA5 data are available at the Copernicus Climate Data Store, https://cds.climate.copernicus.eu (Hersbach et al. 2020). The front and cyclone tracking algorithm is available at https://github.com/ruestefa/storm track (Rüdisühli 2018). The code for the front detection, the calculation of frontal parameters, and the quantile regression is available at https://wegcgitlab.uni-graz.at/ars/INTERACT_code (Schaffer et al. 2024).

References

Barnston, A. G., and R. E. Livezey. 1987. "Classification, Seasonality and Persistence of Low-Frequency Atmospheric Circulation Patterns." *Monthly Weather Review* 115: 1083–1126.

Berry, G., M. J. Reeder, and C. Jakob. 2011. "A Global Climatology of Atmospheric Fronts." *Geophysical Research Letters* 38: L04809.

Bjerknes, J., and H. Solberg. 1922. *Life Cycle of Cyclones and the Polar Front Theory of Atmospheric Circulation*. Cammermeyers Bogh Google-Books-ID: FyW5QAAACAAJ.

Bluestein, H. B. 1992. *Synoptic-Dynamic Meteorology in Midlatitudes: Observations and Theory of Weather Systems*. Taylor & Francis.

Catto, J. L., C. Jakob, G. Berry, and N. Nicholls. 2012. "Relating Global Precipitation to Atmospheric Fronts." *Geophysical Research Letters* 39, no. 10: 2012GL051736. https://doi.org/10.1029/2012GL051736.

Catto, J. L., and S. Pfahl. 2013. "The Importance of Fronts for Extreme Precipitation." *Journal of Geophysical Research: Atmospheres* 118, no. 10: 10,791–10,801.

Dacre, H. F., and S. L. Gray. 2006. "Life-Cycle Simulations of Shallow Frontal Waves and the Impact of Deformation Strain." *Quarterly Journal of the Royal Meteorological Society* 132: 2171–2190.

Dacre, H. F., and S. L. Gray. 2009. "The Spatial Distribution and Evolution Characteristics of North Atlantic Cyclones." *Monthly Weather Review* 137: 99–115.

Davies, H. C. 1999. "Theories of Frontogenesis." In *The Life Cycles of Extratropical Cyclones*, edited by M. A. Shapiro and S. Grønås, 215–238. American Meteorological Society. https://doi.org/10.1007/978-1-935704-09-6_16.

Davies, H. C., and A. M. Rossa. 1998. "PV Frontogenesis and Upper-Tropospheric Fronts." *Monthly Weather Review* 126: 1528–1539.

de Ponce León, S., and C. Guedes Soares. 2014. "Extreme Wave Parameters Under North Atlantic Extratropical Cyclones." *Ocean Modelling* 81: 78–88.

Dowdy, A. J., and J. L. Catto. 2017. "Extreme Weather Caused by Concurrent Cyclone, Front and Thunderstorm Occurrences." *Scientific Reports* 7: 40359.

Easterling, D. R., G. A. Meehl, C. Parmesan, S. A. Changnon, T. R. Karl, and L. O. Mearns. 2000. "Climate Extremes: Observations, Modeling, and Impacts." *Science* 289: 2068–2074.

Feser, F., M. Barcikowska, O. Krueger, F. Schenk, R. Weisse, and L. Xia. 2015. "Storminess Over the North Atlantic and Northwestern Europe—A Review." *Quarterly Journal of the Royal Meteorological Society* 141: 350–382.

Field, P. R., and R. Wood. 2007. "Precipitation and Cloud Structure in Midlatitude Cyclones." *Journal of Climate* 20: 233–254.

Friederichs, P. 2010. "Statistical Downscaling of Extreme Precipitation Events Using Extreme Value Theory." *Extremes* 13: 109–132. https://doi.org/10.1007/s10687-010-0107-5.

Gramcianinov, C. B., R. M. Campos, R. de Camargo, K. I. Hodges, C. Guedes Soares, and P. L. da Silva Dias. 2020. "Analysis of Atlantic Extratropical Storm Tracks Characteristics in 41 Years of ERA5 and CFSR/CFSv2 Databases." *Ocean Engineering* 216: 108111.

Hanley, J., and R. Caballero. 2012. "Objective Identification and Tracking of Multicentre Cyclones in the ERA-Interim Reanalysis Dataset." *Quarterly Journal of the Royal Meteorological Society* 138: 612–625.

Hawcroft, M. K., L. C. Shaffrey, K. I. Hodges, and H. F. Dacre. 2012. "How Much Northern Hemisphere Precipitation is Associated With Extratropical Cyclones?" *Geophysical Research Letters* 39: L24809.

Heitmann, K., M. Sprenger, H. Binder, H. Wernli, and H. Joos. 2024. "Warm Conveyor Belt Characteristics and Impacts Along the Life Cycle of Extratropical Cyclones: Case Studies and Climatological Analysis Based on ERA5." *Weather and Climate Dynamics* 5: 537–557.

Hersbach, H., B. Bell, P. Berrisford, et al. 2020. "The ERA5 Global Reanalysis." *Quarterly Journal of the Royal Meteorological Society* 146: 1999–2049.

Hewson, T. 2009. "Diminutive Frontal Waves—A Link Between Fronts and Cyclones." *Journal of the Atmospheric Sciences* 66: 116–132.

Hewson, T. D. 1998. "Objective Fronts." *Meteorological Applications* 5: 37–65.

Hewson, T. D., and U. Neu. 2015. "Cyclones, Windstorms and the IMILAST Project." *Tellus A: Dynamic Meteorology and Oceanography* 67: 27128. https://doi.org/10.3402/tellusa.v67.27128.

Hoskins, B. J. 1982. "The Mathematical Theory of Frontogenesis." *Annual Review of Fluid Mechanics* 14: 131–151.

Hurrell, J. W., and C. Deser. 2010. "North Atlantic Climate Variability: The Role of the North Atlantic Oscillation." *Journal of Marine Systems* 79: 231–244.

Hurrell, J. W., Y. Kushnir, G. Ottersen, and M. Visbeck. 2003. "An Overview of the North Atlantic Oscillation." In *The North Atlantic Oscillation: Climatic Significance and Environmental Impact*, 1–35. American Geophysical Union (AGU). https://onlinelibrary.wiley.com/doi/pdf/10.1029/134GM01.

Jenkner, J., M. Sprenger, I. Schwenk, C. Schwierz, S. Dierer, and D. Leuenberger. 2010. "Detection and Climatology of Fronts in a High-Resolution Model Reanalysis Over the Alps." *Meteorological Applications* 17: 1–18.

Karwat, A., C. L. E. Franzke, J. G. Pinto, S.-S. Lee, and R. Blender. 2024. "Northern Hemisphere Extratropical Cyclone Clustering in ERA5 Reanalysis and the CESM2 Large Ensemble." *Journal of Climate* 37: 1347–1365.

Koenker, R. 2005. *Quantile Regression. Econometric Society Monographs*. Cambridge University Press. https://www.cambridge.org/core/books/quantile-regression/C18AE7BCF3EC43C16937390D44A328B1.

Koenker, R., and J. A. F. Machado. 1999. "Goodness of Fit and Related Inference Processes for Quantile Regression." *Journal of the American Statistical Association* 94: 1296–1310.

Lackmann, G. 2011. *Midlatitude Synoptic Meteorology: Dynamics, Analysis, and Forecasting*. 1st ed. American Meteorological Society.

Lamb, H. H. 1951. "Essay on Frontogenesis and Frontolysis, Parts I, II and III." *Meteorological Magazine* 80: 35–46.

Lavers, D. A., A. Simmons, F. Vamborg, and M. J. Rodwell. 2022. "An Evaluation of ERA5 Precipitation for Climate Monitoring." *Quarterly Journal of the Royal Meteorological Society* 148: 3152–3165.

Neu, U., M. G. Akperov, N. Bellenbaum, et al. 2013. "IMILAST: A Community Effort to Intercompare Extratropical Cyclone Detection and Tracking Algorithms." *Bulletin of the American Meteorological Society* 94: 529–547.

Owen, L. E., J. L. Catto, D. B. Stephenson, and N. J. Dunstone. 2021. "Compound Precipitation and Wind Extremes Over Europe and Their Relationship to Extratropical Cyclones." *Weather and Climate Extremes* 33: 100342.

Parker, D. J. 1998. "Secondary Frontal Waves in the North Atlantic Region: A Dynamical Perspective of Current Ideas." *Quarterly Journal of the Royal Meteorological Society* 124: 829–856.

Pinto, J., T. Spangehl, U. Ulbrich, and P. Speth. 2005. "Sensitivities of a Cyclone Detection and Tracking Algorithm: Individual Tracks and Climatology." *Meteorologische Zeitschrift* 14: 823–838.

Pinto, J. G., S. Zacharias, A. H. Fink, G. C. Leckebusch, and U. Ulbrich. 2009. "Factors Contributing to the Development of Extreme North Atlantic Cyclones and Their Relationship With the NAO." *Climate Dynamics* 32: 711–737. https://doi.org/10.1007/s00382-008-0396-4.

Priestley, M. D. K., H. F. Dacre, L. C. Shaffrey, S. Schemm, and J. G. Pinto. 2020. "The Role of Secondary Cyclones and Cyclone Families for the North Atlantic Storm Track and Clustering Over Western Europe." *Quarterly Journal of the Royal Meteorological Society* 146: 1184–1205.

Renard, R. J., and L. C. Clarke. 1965. "Experiments in Numerical Objective Frontal Analysis." *Monthly Weather Review* 93: 547–556.

Ritter, R. 2014. *A Novel Front Detection Algorithm Tested in Complex Terrain*. Master's thesis, University of Graz. http://unipub.uni-graz.at/obvugrhs/242774.

Roberts, J. F., A. J. Champion, L. C. Dawkins, et al. 2014. "The XWS Open Access Catalogue of Extreme European Windstorms From 1979 to 2012." *Natural Hazards and Earth System Sciences* 14: 2487–2501.

Rogers, J. C. 1997. "North Atlantic Storm Track Variability and Its Association to the North Atlantic Oscillation and Climate Variability of Northern Europe." *Journal of Climate* 10: 1635–1647.

Rudeva, I., and I. Simmonds. 2015. "Variability and Trends of Global Atmospheric Frontal Activity and Links With Large-Scale Modes of Variability." *Journal of Climate* 28: 3311–3330.

Rüdisühli, S. 2018. *Attribution of Rain to Cyclones and Fronts Over Europe in a Kilometer-Scale Regional Climate Simulation*. Doctoral Thesis. ETH Zurich.

Schaffer, A., T. Lichtenegger, H. Truhetz, A. Ossó, O. Martínez-Alvarado, and D. Maraun. 2024. "Drivers of Cold Frontal Hourly Extreme Precipitation: A Climatological Study Over Europe." *Geophysical Research Letters* 51: e2024GL111025.

Schemm, S., and M. Sprenger. 2015. "Frontal-Wave Cyclogenesis in the North Atlantic—A Climatological Characterisation." *Quarterly Journal of the Royal Meteorological Society* 141: 2989–3005. https://doi.org/10.1002/qj.2584.

Schemm, S., M. Sprenger, O. Martius, H. Wernli, and M. Zimmer. 2017. "Increase in the Number of Extremely Strong Fronts Over Europe? A Study Based on ERA-Interim Reanalysis (1979–2014)." *Geophysical Research Letters* 44: 553–561.

Schemm, S., M. Sprenger, and H. Wernli. 2018. "When During Their Life Cycle Are Extratropical Cyclones Attended by Fronts?" *Bulletin of the American Meteorological Society* 99: 149–165.

Shapiro, M. A. 1990. *Fronts, Jet Streams, and the Tropopause*. U.S. Dept. of Commerce, National Oceanic and Atmospheric Administration, Environmental Research Laboratories, Wave Propagation Laboratory; For sale by the National Technical Information Service.

Simmonds, I., K. Keay, and J. A. T. Bye. 2012. "Identification and Climatology of Southern Hemisphere Mobile Fronts in a Modern Reanalysis." *Journal of Climate* 25: 1945–1962.

Ulbrich, U., G. C. Leckebusch, and J. G. Pinto. 2009. "Extra-Tropical Cyclones in the Present and Future Climate: A Review." *Theoretical and Applied Climatology* 96: 117–131. https://doi.org/10.1007/s00704-008-0083-8.

Wernli, H., and C. Schwierz. 2006. "Surface Cyclones in the ERA-40 Dataset (1958–2001). Part I: Novel Identification Method and Global Climatology." *Journal of the Atmospheric Sciences* 63: 2486–2507.

Supporting Information

Additional supporting information can be found online in the Supporting Information section.